Mine Water and the Environment (2019) 38:166–177
https://doi.org/10.1007/s10230-018-0552-y

TECHNICAL ARTICLE

A Robust Model Coupling Subsidence with Salt Dissolution

Vong Chan Quang[1] · **Sébastien Gourdier**[1] · **Behrooz Bazargan-Sabet**[1,2]

Received: 22 May 2017 / Accepted: 27 June 2018 / Published online: 2 July 2018

Abstract
A robust 3D model of subsidence coupled with channeling into salt formations was developed. Its architecture allows easy implementation of empirical phenomenological laws regarding channel formation and subsidence within a formation. The model can be used to perform fast and adapted-to-complexity computations where data are sparse in time and space and where extensive state-of-the-art measurements are not available; as a preliminary model, it could ideally guide the development of more sophisticated, heavily parameterized and resource-demanding codes. Sensitivity analyzes on several 2D and 3D parameterizations were performed to assess the influence of several parameters in determining the shape of subsidence. The 3D finite element model coupling flow (using Darcy's law) and subsidence (empirical models) was then tested for a French nineteenth century salt mining site, where mining may have induced subsidence by disrupting the balance between fresh water and brine. A sensitivity analysis was conducted to assess the impact of flow parameters or subsidence on results.

Keywords Salt rock · Collapse · 2D/3D modeling

Introduction

In addition to direct surface mechanical instability, salt workings may cause additional subsidence around openings through dissolution of salt strata surrounding the exploitation zones. Prior to mining, the saturated brine is generally in equilibrium within these formations, but the presence of openings results in brine circulation, allowing introduction of fresh water, which leads to dissolution of salt strata, mechanical changes, instabilities and, finally, surface subsidence. This subsidence exhibits different patterns and dynamics depending on the geology of the caprock, from slow compaction to sudden collapse (Waltham et al. 2005). The aim of this study was to simulate this phenomenon, observed inter alia in Nancy Basin (France) since the nineteenth century, by developing a robust three dimensional (3D) coupled model.

Subsidence led by dissolution has been studied in several major sites (e.g. Spain and Jordan). Geochemical modeling of salt dissolution in highly saturated brines is a delicate task (Trémosa et al. 2014), while geochemical modeling in carbonates is better handled with current modeling tools. In both cases, a thorough characterization of general rock properties (porosity, permeability, fracturing) as well as of their spatial variability is critical for a good understanding of the system.

Current state-of-the-art reactive transport models studying geochemical reactions at macroscopic level need a significant amount of data for their parameterization. We were looking to build a model for situations where knowledge is sparse. Our aim was to build a tool for estimating potential surface impact of salt dissolution driven by percolation of fresh water. Using a 3D finite element model that relies on Darcy's law and a simplified equation linking flow, dissolution, and porosity threshold conditions for collapses, we built a model simulating subsidence of a homogeneous clay caprock over salt strata. The rationale of the model, its parameterization, and its results are discussed and compared to a French nineteenth century case (Dombasle, Nancy Basin, France).

✉ Sébastien Gourdier
s.gourdier@brgm.fr

[1] BRGM, 3 Ave Claude Guillemin, BP 36009, 45060 Orléans Cedex 2, France

[2] Université de Lorraine, Campus ARTEM, CS 14 234, 92 rue Sergent Blandan, 54042 Nancy, France

Literature Review

Subsidence driven by dissolution or particle transport due to flow circulation (or water level movement) has been studied at several major sites. In the Dead Sea area, sinkhole hazard is high due to salt dissolution induced by sea level changes and intrusion of brackish waters into salt layers previously in contact with saturated brines. Frumkin et al. (2011) determined the geometry of the salt layers, the variability of porosity and permeability, as well as shallow deformations using seismic refraction, transient electromagnetic method, electrical resistivity tomography, and ground penetration radar. Shalev et al. (2006) established a 2D finite element model of salt dissolution of the Dead Sea shore as a driver of subsidence and collapses. Sensitivity analyses were done on critical geochemical parameters, such as dissolution rates, specific surfaces, porosity–permeability law, dispersivity, geometry, and boundary conditions. The difficulty in using right state equations for simulating brine composition was discussed.

Gutiérrez (2004) discussed the origin of subsidence in the Canyonlands (Colorado Plateau, USA) and concluded that the main mechanism causing large-scale subsidence of the site was dissolution of the salt anticlines and valleys rather than tectonic subsidence. Other case studies include paleo-collapses in rivers due to evaporite dissolution in Spain (Guerrero et al. 2008) and paleo-sinkholes due to interstrata halite dissolution at the La Loleta Dam (Gutiérrez et al. 2015).

Several models of limestone karstification have been published. The model of calcite geochemistry generally used for karst models was described by Kaufmann and Dreybrodt (2007), while carbonate geochemistry in general was described by Appelo and Postma (2005). Hiller et al. (2011) modelled karstification around a dam in 3D using finite elements. An initial fracture network was built representing fractures as tubes with diameters that followed a statistical distribution. The dissolution mechanism leading to enlargement of the fractures was computed each time-step through a relationship based on the flux rate. This model was applied to the Birs weir dam site (Switzerland), accounting for vertical fluxes like rainfall. Zidane et al. (2014) tested the influence of several subsurface parameters (boundary conditions, hydraulic conductivity, aquifer geometry, and geometry of faults) on the dynamics of evaporate dissolution in a coupled flow and transport model, and showed the influence of fault geometry, and that Darcy's equations are not relevant when large voids are considered.

Subsidence of the Harz Mountains (Germany) was studied by Kaufmann and Romanov (2016). Anhydrite karstification was modeled and collapse was simulated based on a mechanical instability criterion that updates fracture diameters and creates voids. This model was compared to geophysical measurements (magnetic, self-potential, electrical resistivity tomography). A comprehensive review of the engineering aspects of karst subsidence can be found in Waltham et al. (2005). Another thorough review of karst subsidence issues (as well as flood and slope movements) provides an inventory of the mechanisms involved, explains the strategies for susceptibility/hazard mapping, and sums up directions for future investigations (Gutiérrez et al. 2014). Non-linear models and spatially heterogeneous/anisotropic property modeling have also been successfully used in other fields (e.g. Valipour 2016; Viero and Valipour 2017).

Rationale for a Robust Model

Linking transport and geochemistry to subsidence is a challenging issue for modelers. Competition between geochemical phenomena (precipitation, dissolution, sorption, exchange, etc.) and geomechanical phenomena is complex, with each of these phenomena leading to, at a minimum, porosity and pressure changes. The very complex topic of this interplay has been theoretically studied by Malvoisin et al. (2015). Reactive transport models are required if one wants to accurately model geochemical reactions at the macroscopic level. However, such models demand a significant amount of data (exhaustive water and mineral compositions, experimental kinetic laws, specific surfaces, etc.). In most of the reviewed work, the authors directly set up geochemical equations for either calcite or salt exclusively, taking the safe and legitimate assumption that in the specific context of their studies, these elements are the overwhelming drivers of the phenomena. However, theoretically, a fully exhaustive geochemical model requires a complete analysis of major and minor aqueous species, as well as a complete mineralogical analysis including spatial variability at the desired modeling scale, which leads, in general, to the introduction of other minerals into the model and may cause competition among possible mechanisms.

Numerical dispersion is unavoidable in advection–diffusion models and can be a major or minor issue depending on the setup trade-offs behind the transport model. Furthermore, modeling the behavior of highly saline waters is challenging (Trémosa et al. 2014), especially in complex mineralogical contexts, requiring the use of Pitzer equations as well as the corresponding databases, instead of those used for more dilute solutions.

Aside from linking fluid flow and geochemistry to standard mechanical models (e.g. poro-elastoplasticity), the other modeling challenge is how to express subsidence, which takes a great variety of shapes and dynamics. Large

collapses may happen unexpectedly, as well as very slow deformations. The subsurface geology has a strong influence in this dynamic as, for example, a carbonate layer that can keep the surface from collapsing until stresses become overwhelming. Considering the difficulty in handling this phenomenon at the pore level and to model subsidence, we took a macroscopic and empirical approach. In general, for a certain spatial/time resolution and for a defined problem, one should select a model with an appropriate level of sophistication. For situations where knowledge is sparse in time and space and where stakes are relatively low, a robust model is, at least for a preliminary study, more relevant than an over-parameterized one that will be costly and will actually rely on large uncertainties. The requirements for such a robust and simplified model are:

- It must be adapted to the purpose of the study (e.g. mapping risk with a given degree of precision in time and space);
- it must be adapted to the level of knowledge and available field data. In many cases, only broad knowledge is available, such as global hydrological circulation, global/approximate rock properties, and geometries;
- it should help explain observations and limit the number of alternative configurations;
- it gives guidance for more sophisticated modeling tools as further knowledge is progressively gathered.

In order to build such a robust model, we introduce the following strong assumptions:

- We consider salt strata covered by a relatively shallow layer of clay with a simplified deformation mechanism governed by gravity;
- although other approaches, such as subsidence in compressible sediments (studied by Mahmoudpour et al. 2016) may be relevant, we make the assumption that, over a long span of time, collapses are the most significant part of deformations;
- collapses are triggered by salt dissolution through freshwater percolation. The model will represent this by considering porosity changes under flow, and link deformations to porosity and flow conditions;
- fluid flow follows Darcy's Law;
- dissolution leads to channel formation due to the heterogeneity of the salt layer;
- salt dissolution is modeled by porosity changes linked to flow circulation and constrained by the distribution of soluble and insoluble components and voids;
- subsidence is modeled by redistribution of soluble and insoluble components and voids triggered by a condition on porosity;
- a macroscopic approach is taken; faulting and cracking are not considered.

Model of Subsidence Linked to Water Circulation

Darcy's Law

We consider that Darcy's Law is suitable for our macroscopic approach. In the domain Ω with contour $\partial\Omega$, Darcy's law reads:

$$\vec{v} = -\frac{\kappa}{\mu}\left(\nabla p + \rho\vec{g}\right) \tag{1}$$

$$\frac{\partial(\rho\varphi)}{\partial t} + \mathrm{div}\rho\vec{v} = \Phi \tag{2}$$

$$\vec{n}\cdot\vec{v} = \Psi \tag{3}$$

where $\vec{v}$ is Darcy velocity, κ is the permeability, μ is the viscosity, p is the pressure, ρ is the fluid density, $\vec{g}$ is the gravity vector, φ is the porosity, Φ is the source term, Ψ is the flux term, and $\vec{n}$ is the vector normal to $\partial\Omega$.

Trial and test functions, in the mixed variational form of Darcy's law, are defined in Brezzi–Douglas–Marini (Arnold et al. 2002) and discontinuous Galerkin spaces $\mathbf{V}$ and $\mathbf{P}$. For $V = (\vec{v}, p)$ and all $W = (\vec{w}, q)$ in $\mathbf{V}\times\mathbf{P}$, the bilinear formulation B and the linear formulation L of Darcy's law are, respectively:

$$B(W,V) = \left(\vec{v}, \frac{\mu}{\kappa}\vec{v}\right) - (\mathrm{div}\vec{w}, p) + (q, \mathrm{div}\vec{v}) \tag{4}$$

$$L(W) = \left(\vec{w}, \frac{\rho}{g_c}\vec{g}\right) + (q,\Phi) - \left(\frac{\partial\varphi}{\partial t}, q\right) - (p\vec{n}, \vec{w}) \tag{5}$$

The last term represents Dirichlet boundary conditions in pressures that are enforced directly into the variational formulation. Solving this problem means finding V such that for all values of W:

$$B(W,V) = L(W) \tag{6}$$

For this subsidence-oriented model, no transport of dissolved species was simulated. However, transport laws should be implemented if environmental impact (e.g. pollution) is an issue.

Salt Dissolution Law

To implement a simplified representation of geochemical phenomena, meeting the criteria set out previously (cf. 3), the model relies on formulation of porosity variation

adapted from an erosion law that Yao et al. (2012) used to model channel formations:

$$\frac{\partial \varphi}{\partial t} = \xi(1-\varphi) \parallel \vec{v} \parallel \tag{7}$$

where $\vec{v}$ is Darcy velocity in m s^{-1} and φ is the porosity. We set $\xi = kc$, where c is the salt concentration in the brine (mol m^{-3}) and k is a factor in m^2 mol^{-1}. The influence of ξ on modeling results is decisive, as we shall see further (cf. 5.2.1). Other formulations should be considered if the transport law is implemented. Simplifying the geochemical phenomena, we attribute three volume fractions to each element:

- p: voids (porosity), through which water flows;
- s: soluble rock; and
- i: insoluble rock, which may be originally included in the salt layer, or come from the caprock when subsidence occurs.

The three parameters are linked by the equation:

$$p + i + s = 1 \tag{8}$$

The amount of soluble rock constrains the maximum possible channel formation (porosity augmentation) due to flow and salt dissolution.

Porosity–Permeability Law

We used a cubic law commonly applied in reactive transport modeling to link porosity to permeability, as in Shalev et al. (2006), with $n = 3$. The link between porosity and permeability is actually highly complex, so improvements were made using the models proposed by Nelson et al. (1994), for example.

$$\kappa = \kappa_0 \left(\frac{\varphi}{\varphi_0} \right)^3 \tag{9}$$

where φ is the porosity, κ is the permeability, φ_0 is the reference porosity, and κ_0 is the reference permeability.

Subsidence

Subsidence is modeled with redistribution of the void, soluble, and insoluble volumes, using a threshold condition on porosity as well as redistribution parameters. We used the following two models.

Full Column Vertical Translation

In this model (Fig. 1, left), if porosity in an elementary volume increases above a determined threshold, the whole column is repositioned by the volume represented by the

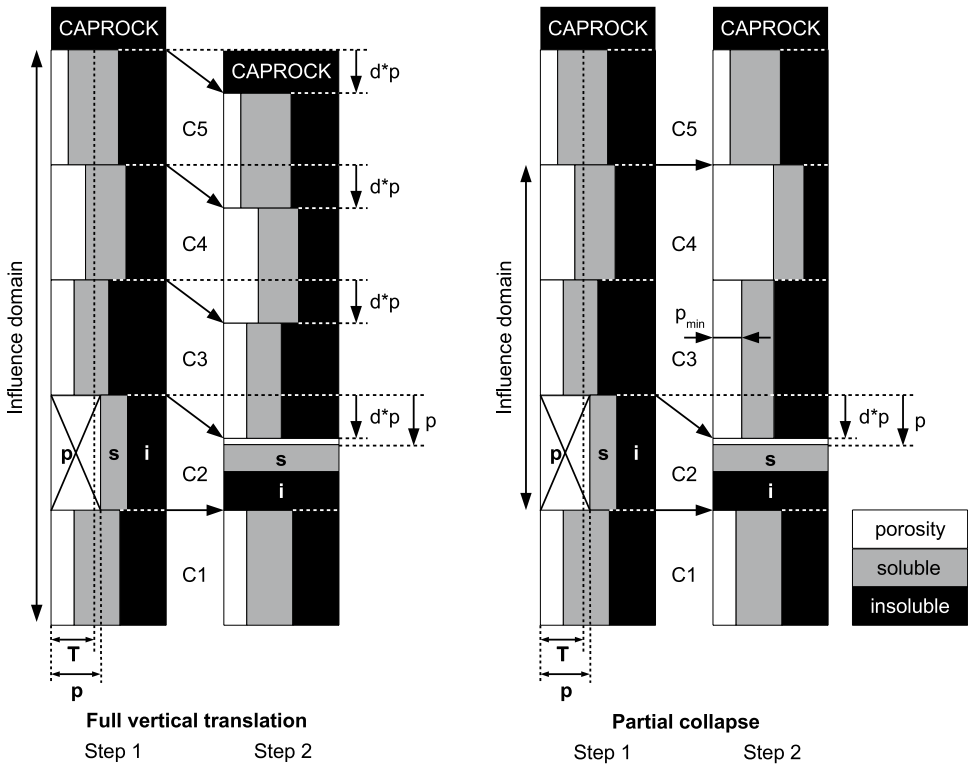

Fig. 1 Models of subsidence: full vertical translation of a column of cells (left) and redistribution of volumes over a predefined influence distance (right)

porosity p of the element multiplied by an expansion factor d (to account for the collapsed materials that will not be fully compacted). The column consists of five cells, each cell being divided into the porosity (p), soluble material (s), and insoluble material (i) volume fraction. In step 1, cells triggering subsidence are identified: e.g., in cell 2, p exceeds the porosity threshold T and triggers subsidence. Subsidence affects the whole column above cell 2 (cells 2, 3, 4, and 5). The porosity threshold T is a parameter of the model, which has to be estimated from observations.

In step 2, the map of p, s, and i is updated for each cell based on vertical translation of the affected part of the column. The maximum volume fraction of cell 3 allowed to be introduced into cell 2 is p, but due to the expansion factor, $d \times p$ fraction of each cell N is translated into cell $N-1$. On top of the column, the caprock (assumed to be 100% insoluble) is introduced. The actual displacement of the column is $d \times p \times dim_Z$, where dim_Z is the vertical dimension of the cell that triggered the subsidence.

Partial Collapse

Because mechanical stresses can actually preserve the cohesion of the structure above a certain distance from the collapse, we also tested a model (Fig. 1, right) where displacements are limited to a certain distance above the weakened element. This column consists of five cells. As in the previous case in step 1, cell 2 triggers subsidence when porosity p exceeds the threshold. The subsidence partially affects the column above cell 2 over a predefined influence distance (cells 2, 3, and 4).

In step 2, the map of p, s, and i is updated for each cell, based on vertical translation of the bottom of the affected part of the column and on the total contributions of p, s, and i within the influenced domain. The actual displacement of the bottom of the column is $d \times p \times dim_Z$, but in the lower cells of the influenced domain, a porosity p_{min} is imposed. In the top of the influenced domain (cell 4 here), p, s, and i are determined so that the total contribution (cells 2, 3, and 4) of p, s, and i is kept equal from step 1 to step 2.

Application to a Subsidence Case Related to Salt Mining: The Case of Dombasle, France, 1850-Today

Case Description

In the area of Dombasle (near Nancy, France), the subsurface consists of an important Lower Keuper saliferous sedimentary deposit, made of interbedded claystone and salt rock with a variable amount of insoluble material, approximately 200 km long, 50 km wide, and 100–150 m thick, with a dip of a few degrees (Saunier and Courrioux 2008). This saliferous deposit is covered by layers of sandstone, marls, and claystone (Fig. 2). Under river beds, the saliferous formation roof is only 50 m deep.

The dissolution mechanism is likely related to rainwater percolation through the overburden towards the salt deposit, the former having a higher hydraulic conductivity. Some of the groundwater flows towards outlets (springs or rivers) after having leached the top of the saliferous layers. The rest infiltrates through the salt deposit and flows through it, dissolving the salt (Fig. 2).

The salt deposit was industrially mined for 150 years in Nancy Basin at the confluence of the Meurthe and Sânon rivers, 12 km south-east of Nancy. Mining probably accelerated groundwater flow from the overburden to the salt

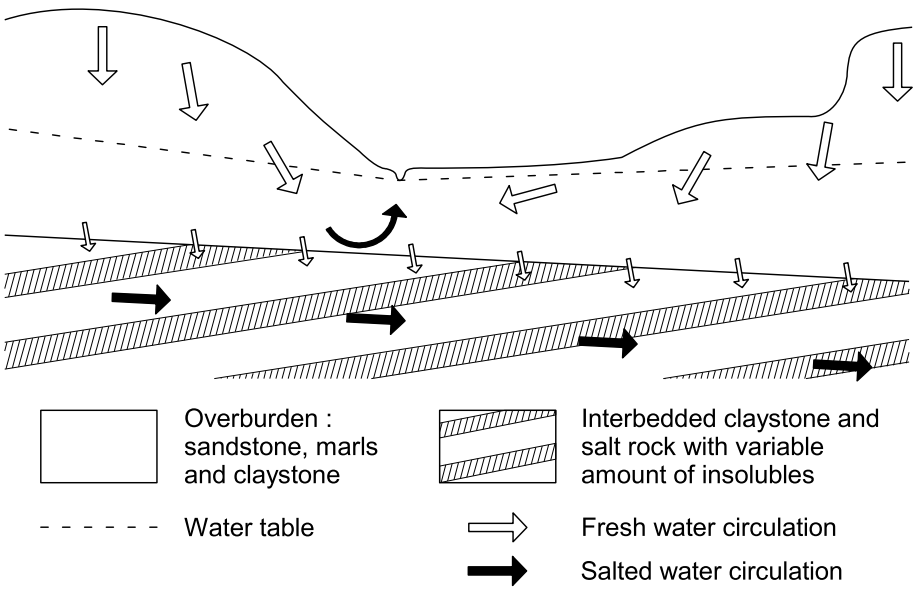

Fig. 2 A lithostratigraphic section of the Dombasle aquifer

deposit and through it. Subsidence rates have been measured between 30 and 60 mm/year during active dissolution periods and could reach 140 mm/year. During low dissolution periods, the subsidence rate is only about 5 mm/year. Cumulative subsidence after 70 years is approximately 1 m in several sectors and has exceeded 2 m at some locations.

The model described above was used in 2D and 3D to simulate groundwater flow in the salt deposit and the resulting subsidence observed at the surface. We used the open source finite element software FEniCS (Alnæs et al. 2015). The simulations and sensitivity analyses were first performed in 2D to assess the value of parameter ξ of the ordinary differential equation describing salt dissolution, and then was extended to the 3D model.

2D Modeling

To adjust the parameters, we first considered a 200 m × 50 m 2D model with 20,000 elements in a grid determined by 1 m × 1 m unit cells. Simulations were performed for t = 50 years. The boundary conditions were:

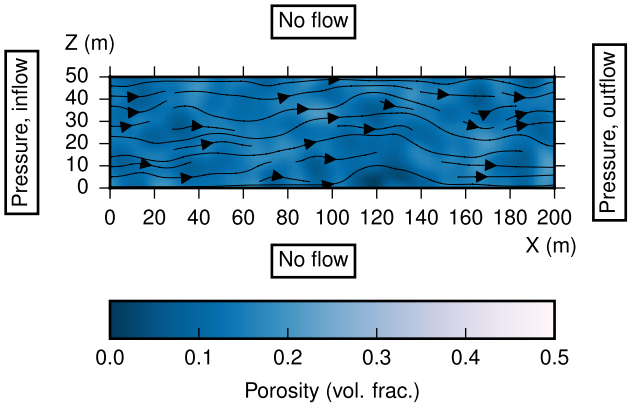

Fig. 3 A 2D model with initial heterogeneous porosity field and boundary conditions

- Dirichlet conditions in pressure were enforced at both lateral sides so that the hydraulic gradient was 0.4%;
- Neumann conditions for Darcy flow constrained the ceiling and floor as no-flow boundary conditions; and
- inflow and outflow were allowed at X = 0 m and X = 200 m.

In order to generate preferential pathways in heterogeneous situations, we set up the initial porosity field by using a Weibull distribution (with parameters shape = 5 and mean = 0.15), with an approximate spatial variability of 10 m. Values of porosity were allowed to vary between ϕ = 0.013 and ϕ = 0.22. We completed this scheme with a homogeneous distribution of insoluble materials representing 50% in volume in the whole domain. Initial porosity, Darcy velocity fields, as well as boundary conditions, are shown in Fig. 3. From this initial state, several 2D simulations were performed to assess the influence of parameter ξ and to compare the two subsidence models (full vertical translation and partial collapse). A time step of 0.5 years was used for all simulations.

Influence of Parameter ξ

The following parameters (Table 1) were used for the sensitivity analysis of parameter ξ. Three values of ξ were tested: 10^{-6}, 2×10^{-6}, and 5×10^{-6}. All three simulations were performed with the same subsidence model: full vertical translation with a threshold value of 0.3 and an expansion factor of 0.8. Porosity maps after 50 years and total variations of porosity, soluble, and insoluble volumes are shown in Fig. 4.

Figure 4 shows that $\xi = 10^{-6}$ (simulation a) was the most realistic case for the Nancy basin subsidence when using the full vertical translation subsidence model. The final ground level is much lower in simulation c than in b. Indeed once all of the soluble material has been evacuated, the subsidence is determined by the amount of insoluble material as well as how porosity is distributed in the final state. Using

Table 1 Simulation parameters

Simulation ID	ξ	Subsidence type	Subsidence parameters	Time (years)
(a)	10^{-6}	Full translation	Threshold = 0.3, expansion = 0.8	50
(b)	2×10^{-6}	Full translation	Threshold = 0.3, expansion = 0.8	50
(c)	5×10^{-6}	Full translation	Threshold = 0.3, expansion = 0.8	50
(d)	10^{-6}	Partial collapse	Threshold = 0.3, expansion = 0.8 Lower porosity = 0.1, infl. dist. = 6 m	100
(e)	10^{-6}	Partial collapse	Threshold = 0.4, expansion = 0.6 Lower porosity = 0.1, infl. dist. = 6 m	100
(f)	10^{-6}	Full translation	Threshold = 0.3, expansion = 0.8	100
(g)	10^{-6}	Full translation	Threshold = 0.4, expansion = 0.6	100
(h)	10^{-6}	Partial collapse	Threshold = 0.3, expansion = 0.8 Lower porosity = 0.1, infl. dist. = 6 m	100
(i)	10^{-6}	Full translation	Threshold = 0.3, Expansion = 0.8	100

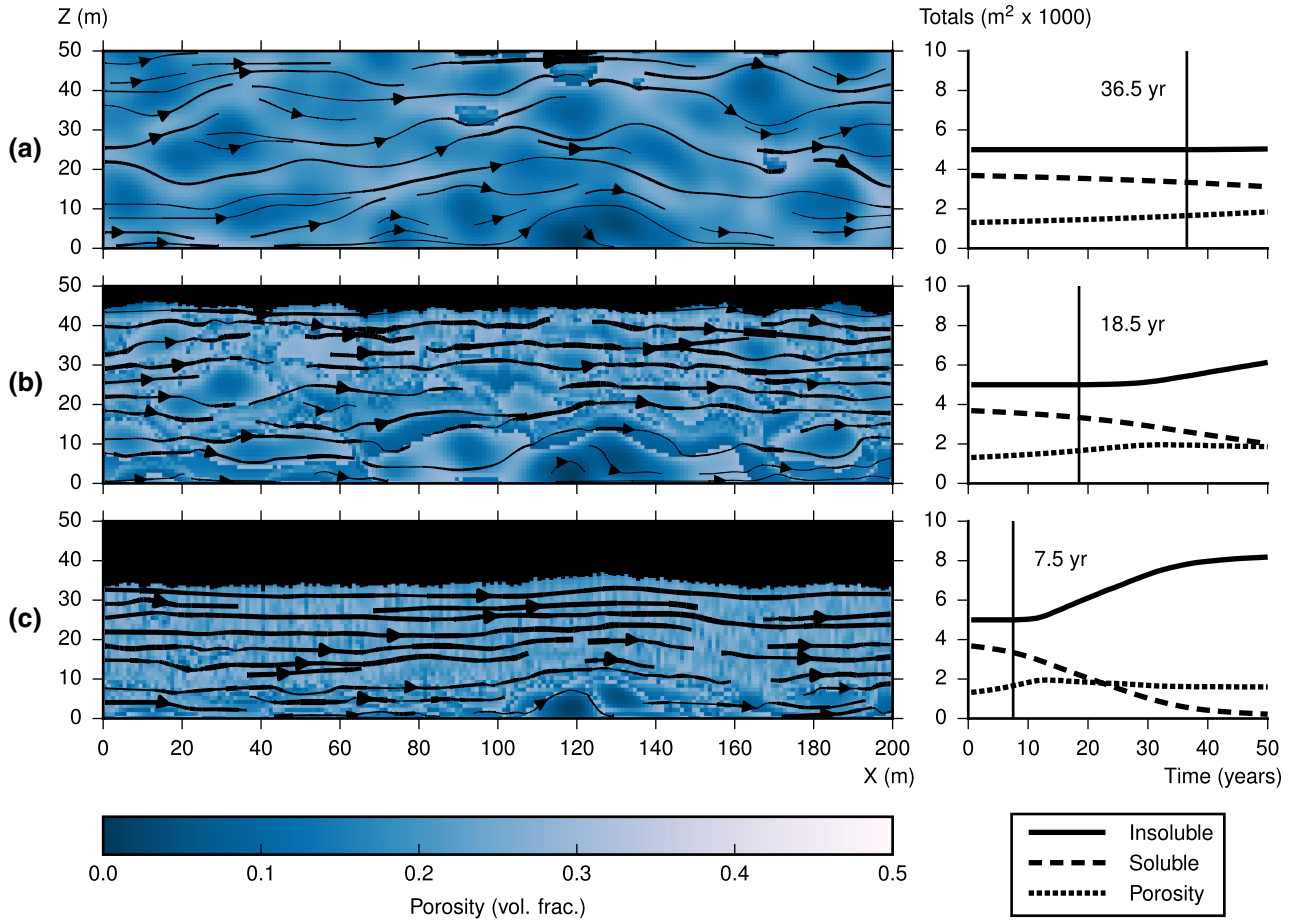

Fig. 4 Porosity field, Darcy velocity field, and subsidence at T = 50 years (left). Evolution of the total volumes of insoluble and soluble materials and porosity contained in the 2D domain (right). The first subsidence event is marked by a vertical line. Sensitivity analysis of parameter ξ for simulations **a**–**c** using parameters from Table 1. Darcy velocity streamlines. The thicker the line, the higher the velocity (scale not harmonized between figures)

a heterogeneous distribution of insoluble material (whether correlated or not to the distribution of porosity) could probably lead to higher ground levels in the final stages. The porosity threshold condition prevents global porosity from growing, as shown in curves b and c in Fig. 4. Porosity reaches a maximum at 30 and 12 years, respectively, when subsidence is triggered. In c, almost all of the soluble rocks are dissolved by the end of the simulation, leaving significant porosity because of the imperfect expansion hypothesis introduced in the subsidence model. With the settings of these simulations, and with the strong hypothesizes taken for this model (including constant gradient and the absence of the mechanical behavior of the caprock), the evolution of the soluble volume is steady.

Comparison of Subsidence Models

In a second series of simulations (d–g), we assessed the influence of the subsidence model. Setting $\xi = 10^{-6}$, we extended the simulation time to 100 years to show the trends more clearly. Table 1 shows the values of the parameters for each simulation. Figure 5 shows that the partial collapse model leads to heavily disturbed configurations, since each time a collapse occurs, the material is totally redistributed, with most of the solids in the lower part and a high void volume at the top. We used a constant influence distance for the collapse, which is why Fig. 5e shows the formation of channels separated by this same distance. A variation of the partial collapse model could be performed using a variable influence distance, as well as by introducing a delay mechanism.

Figure 5 shows that the two different parameterizations d and e of the partial collapse model do not lead to significantly different subsidence amplitudes (geometrically speaking), but the second parameterization e leads to faster dissolution (an earlier decrease in soluble volumes) and higher remaining porosity. The same remarks apply to the alternative full translation model (Fig. 5f, g).

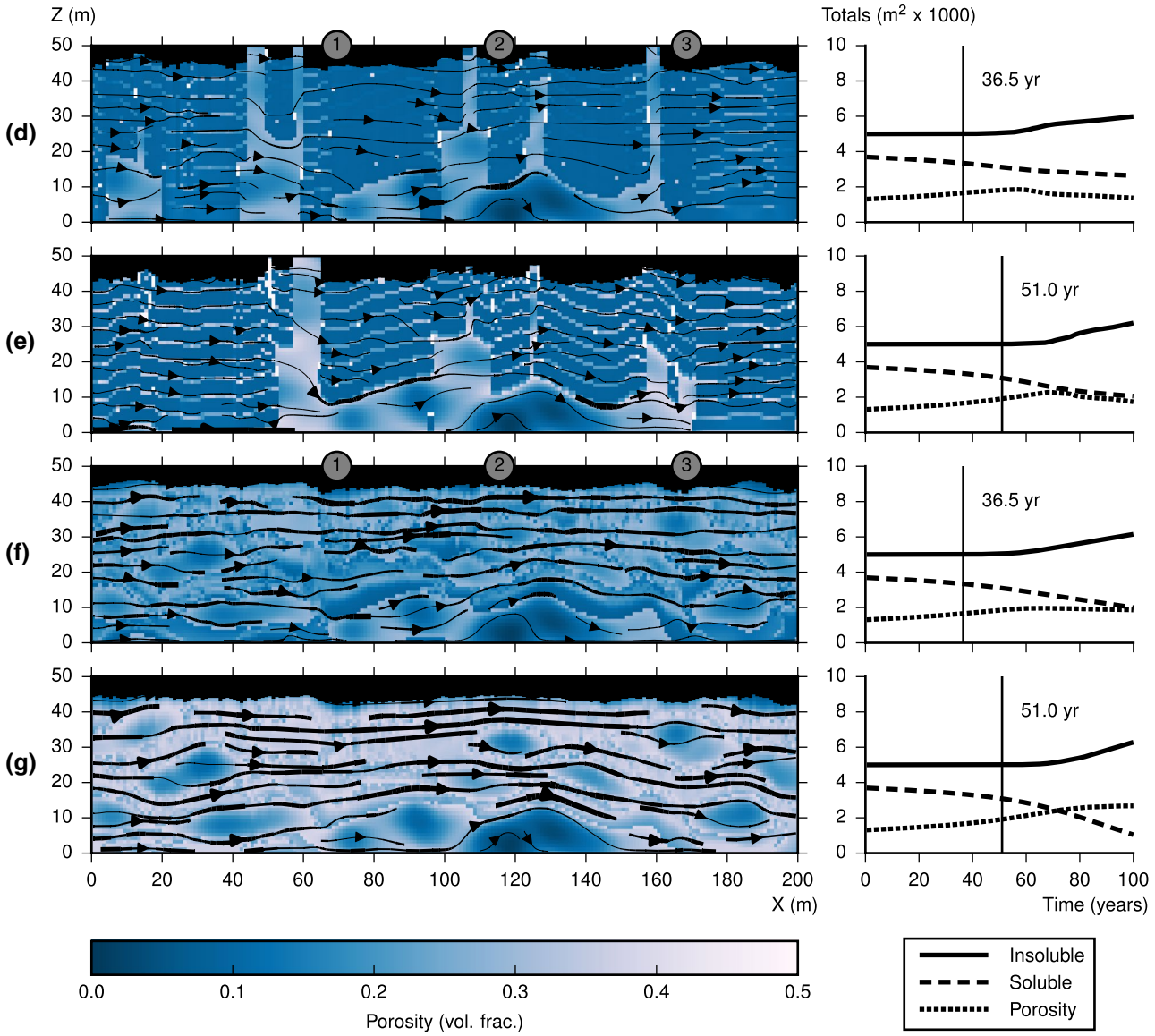

Fig. 5 Porosity field, Darcy velocity field, and subsidence at T = 100 years (left). Evolution of the total volumes of insoluble and soluble materials and porosity contained in the 2D domain (right). The first subsidence event is marked by a vertical line. Sensitivity analysis on the subsidence model. Simulations **d**–**g** using parameters from Table 1. Darcy velocity streamlines. The thicker the line, the higher the velocity (scale not harmonized between figures). In d and f, positions where subsidence time series are analyzed (cf. 5.3 and Fig. 9) are represented by marks ①, ②, and ③

3D Subsidence Model

In the 3D model, the domain is 80 m × 40 m × 10 m in size, with 24,000 elements defined by 2 m × 2 m × 2 m cells. Simulations were performed to model a period of 100 years. The dissolution coefficient $\xi = 10^{-6}$ was used because it was the most realistic parameter in the 2D simulations in conjunction with both subsidence models. As with the 2D model, a heterogeneous distribution of porosity was initially set. Values of porosity were varied between $\phi = 0.05$ and $\phi = 0.23$. As with the 2D model, boundary conditions were:

- Dirichlet pressure conditions were enforced at both faces X = 0 m and X = 80 m, so that the hydraulic gradient was 0.4%;
- Neumann conditions for Darcy flow constrained the ceiling, floor (respectively Z = 0 m and Z = 10 m) and longitudinal sides (Y = 0 m and Y = 40 m) as no-flow boundary conditions.

The initial porosity field, Darcian velocity field, as well as boundary conditions, are shown in Fig. 6. Two simulations were performed to assess the influence of

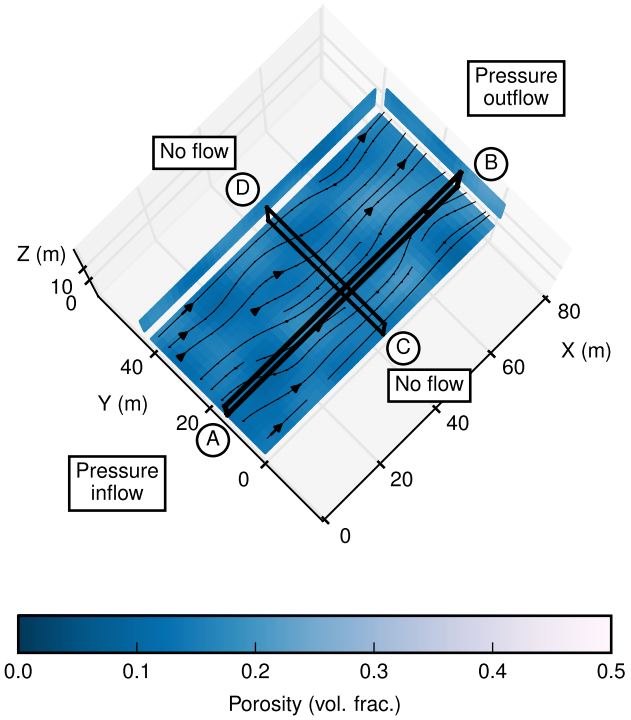

Fig. 6 A 3D model with initial heterogeneous porosity field and boundary conditions. Sections A–B at Y = 12 m and C–D at X = 40 m

the subsidence model. The 3D simulation parameters are shown in Table 1.

The results of the two simulations at 100 years are shown in Figs. 7 and 8. The 3D simulations show the horizontal XY subsidence maps and how the heterogeneity of the formation is translated at the surface. Over 100 years, the two subsidence models differ slightly in terms of the maximum subsidence (2.5 m for the partial collapse model h, and 2.9 m for the full translation model i) and total variations in material (less soluble material is dissolved in model h than in model i). Figures 7 and 8 shows that subsidence as well as the Darcian velocity vary between simulations h and i, which is coherent with the fact that in i, the whole column, from the collapsing cell to the surface, is displaced downward, while in h, only partial collapses are modeled, leaving the surface partly unaffected, according to the influence distance of 6 m.

Subsidence starts in the 3D model approximately 7 years earlier than in the 2D model, presumably because the initial porosity fields were different in 2D and 3D and because adding the third dimension makes flow patterns more complex. As with the 2D models, as soon as subsidence is triggered, the increase of total porosity is stopped. Porosity then decreases monotonously, as does the total volume of soluble materials.

Comparison to Observations

Figure 9 shows a comparison between the observed subsidence in Dombasle (where topographic monitoring has been carried out since the end of the nineteenth century) with simulated subsidence time series, extracted from the 2D (simulations d and f) and 3D models (simulations h and i). The first subsidence cases observed in Dombasle occurred around 1910, 30–40 years after salt mining started in the Dombasle area (1877). The model results are consistent: with $\xi = 10^{-6}$, the first subsidence event occurs after 37 years (Figs. 4, 5).

Observed cumulative subsidence stabilizes between 1 and 2 m (Fig. 9) between the 1950s and 1980s, after 70–100 years of mining. Subsidence rates vary between 30 and 60 mm/year during active dissolution periods and about 5 mm/year during low dissolution period; mean rates vary between 20 and 30 mm/year.

Simulated subsidence after 100 years exceeds 2.5 m in 2D without stabilization, whereas in 3D it stabilizes at about 2 m after 70–90 years. Simulated mean subsidence rates in 2D range between 60 and 120 mm/year. In 3D, simulated mean subsidence rates vary between 30 and 40 mm/year (60 mm/year in one case).

2D simulations obviously overestimate subsidence amplitude, while 3D simulations are closer to actual observations. This is due to several differences: (1) there were more soluble materials in the 50 m thick 2D model than in the 10 m thick 3D model; (2) the simulated flows are more realistic in 3D, since the lateral component is considered in addition to the vertical component. The 3D model parameterization can reproduce the observed start time and subsidence rates. We assumed 100 years of constant exploitation with steady groundwater flow; however, modeling several salt exploitation phases involving different groundwater flows would improve the modeling of the subsidence dynamics. Moreover, as we compared surface observations with subsidence at the top of a salt layer model, we neglected the complex mechanical effects involving the caprock: among other effects, caprock resilience may delay subsidence until breakage, leading to sequences of subsidence phases at varying speeds.

Conclusion

A robust 3D subsidence model coupled with channeling into salt formations was developed. Its architecture allows easy implementation of empirical phenomenological laws (channel formations and subsidence within a formation). The model is intended to perform fast and adapted-to-complexity computations for cases where data are sparse in time and space, and where extensive state-of-the-art

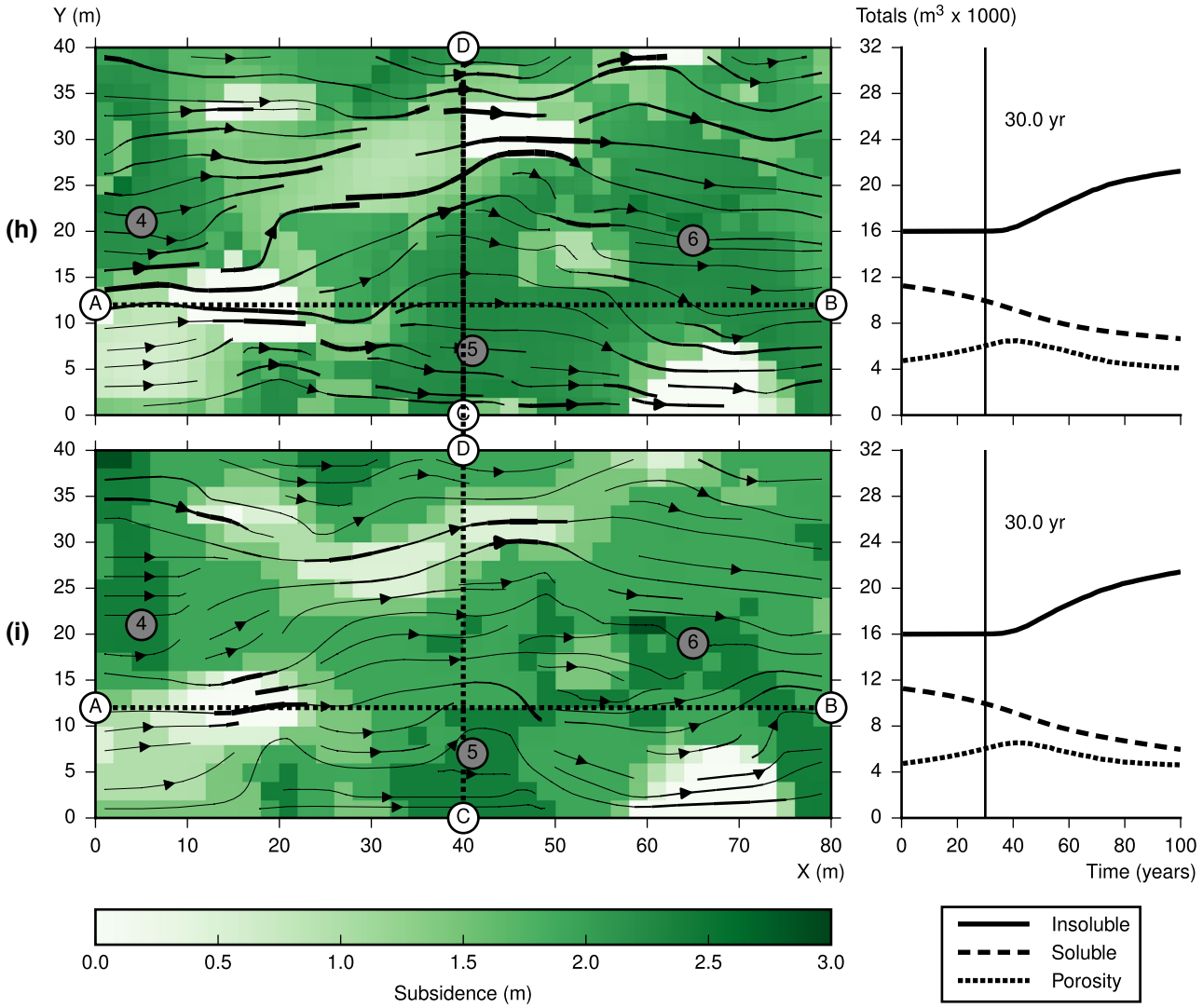

Fig. 7 Darcy velocity field and subsidence at T = 100 years (left). Horizontal XY view; Darcy velocity field at Z = 9 m. Evolution of the total volumes of insoluble and soluble materials and porosity contained in the 3D domain (right). The first subsidence event is marked by a vertical line. Sensitivity analysis on the subsidence model. Simulations h and i using parameters from Table 1. Slices A–B and C–D are shown in Fig. 8. Darcy velocity streamlines. The thicker the line, the higher the velocity (scale not harmonized between figures). In **h** and **i**, positions where subsidence time series are analyzed (cf. 5.3 and Fig. 9) are represented by marks ④, ⑤, and ⑥

measurements are not available; it could ideally guide the development of more sophisticated, heavily parameterized, and resource-demanding codes as a preliminary model.

Sensitivity analyzes on several 2D and 3D parameterizations were performed to assess the influence of several parameters in determining the shape of the subsidence. The results of the 3D model agreed well with the Dombasle case study data in terms of start times and subsidence rates. Improvements can be made by implementing seasonal variations, introducing local influxes of freshwater, or adding geochemical features compatible with a robust model (e.g. influence of temperature).

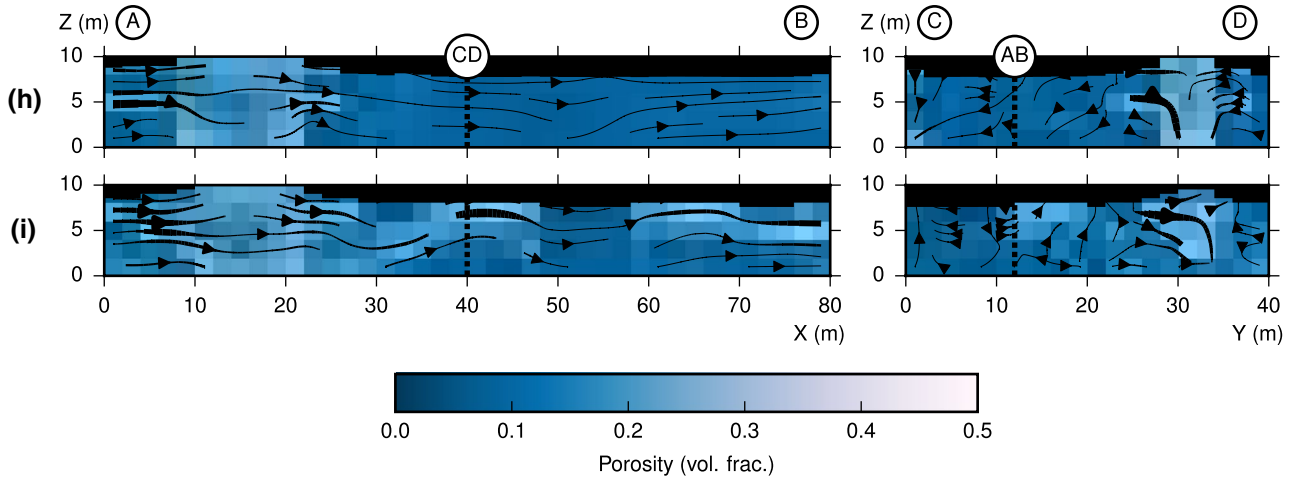

Fig. 8 Porosity field, Darcy velocity field, and subsidence at T = 100 years for sections A–B at Y = 12 m and C–D at X = 40 m (cf. Figs. 6, 7). Sensitivity analysis on the subsidence model. Simulations **h** and **i** using parameters from Table 1. Darcy velocity streamlines. The thicker the line, the higher the velocity (scale not harmonized between figures)

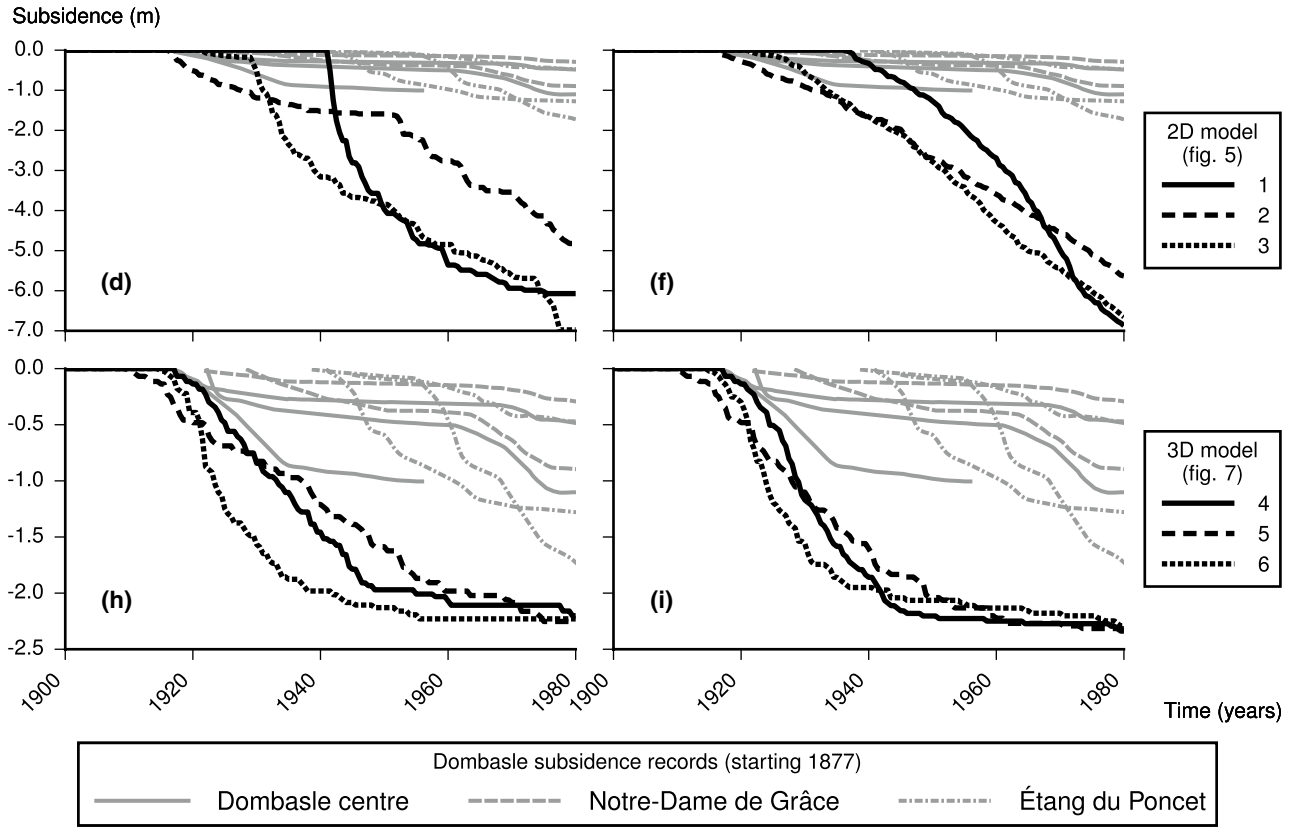

Fig. 9 Observed vs. simulated subsidence. Observations from topographic survey in Dombasle. Simulations **d, f, h**, and **i** using parameters from Table 1. Simulation start time set in the year 1877, when Dombasle salt mining began. Positions where time series are picked are shown on Fig. 5 (2D) and Fig. 7 (3D). We represent the mean subsidence within 5 m of the selected position

References

Alnæs MS, Blechta J, Hake J, Johansson A, Kehlet B, Logg A, Richardson C, Ring J, Rognes ME, Wells GN (2015) The FEniCS project version 1.5. Arch Numer Softw. https://doi.org/10.11588/ans.2015.100.20553

Appelo CAJ, Postma D (2005) Geochemistry, groundwater and pollution, 2nd edn. CRC Press, Taylor & Francis, Boca Raton

Arnold DN, Brezzi F, Cockburn B, Marini LD (2002) Unified analysis of discontinuous Galerkin methods for elliptic problems. SIAM J Numer Anal 39:1749–1779

Frumkin A, Ezersky M, Al-Zoubi A, Akkawi E, Abueladas AR (2011) The Dead Sea sinkhole hazard: geophysical assessment of salt dissolution and collapse. Geomorphology 134:102–117

Guerrero J, Gutiérrez F, Lucha P (2008) Impact of halite dissolution subsidence on Quaternary fluvial terrace development: case study of the Huerva River, Ebro Basin, NE Spain. Geomorphology 100:164–179

Gutiérrez F (2004) Origin of the salt valleys in the Canyonlands section of the Colorado Plateau. Geomorphology 57:423–435

Gutiérrez F, Parise M, De Waele J, Jourde H (2014) A review on natural and human-induced geohazards and impacts in karst. Earth Sci Rev 138:61–88

Gutiérrez F, Mozafari M, Carbonel D, Gómez R, Raeisi E (2015) Leakage problems in dams built on evaporites. The case of La Loteta Dam (NE Spain), a reservoir in a large karstic depression generated by interstratal salt dissolution. Eng Geol 185:139–154

Hiller T, Kaufmann G, Romanov D (2011) Karstification beneath dam-sites: from conceptual models to realistic scenarios. J Hydrol 398:202–211

Kaufmann G, Dreybrodt W (2007) Calcite dissolution kinetics in the system $CaCO_3$–H_2O–CO_2 at high undersaturation. Geochim Cosmochim Acta 71:1398–1410

Kaufmann G, Romanov D (2016) Structure and evolution of collapse sinkholes: combined interpretation from physico-chemical modelling and geophysical field work. J Hydrol 540:688–698

Mahmoudpour M, Khamehchiyan M, Nikudel MR, Ghassemi MR (2016) Numerical simulation and prediction of regional land subsidence caused by groundwater exploitation in the southwest plain of Tehran, Iran. Eng Geol 201:6–28

Malvoisin B, Podladchikov YY, Vrijmoed JC (2015) Coupling changes in densities and porosity to fluid pressure variations in reactive porous fluid flow: local thermodynamic equilibrium: reacting porosity waves. Geochem Geophys Geosyst 16:4362–4387

Nelson PH (1994) Permeability–porosity relationships in sedimentary rocks. Log Anal 35(03):38–62

Saunier M, Courrioux G (2008) Synthèse géologique du bassin salifère de Dombasle (Meurthe-et-Moselle). Final report BRGM/RP-56501-FR

Shalev E, Lyakhovsky V, Yechieli Y (2006) Salt dissolution and sinkhole formation along the Dead Sea shore: salt dissolution and sinkholes. J Geophys Res Solid Earth. https://doi.org/10.1029/2005JB004038

Trémosa J, Castillo C, Vong CQ, Kervévan C, Lassin A, Audigane P (2014) Long-term assessment of geochemical reactivity of CO_2 storage in highly saline aquifers: application to Ketzin, In Salah and Snøhvit storage sites. Int J Greenh Gas Control 20:2–26

Valipour M (2016) How much meteorological information is necessary to achieve reliable accuracy for rainfall estimations? Agriculture 6:53. https://doi.org/10.3390/agriculture6040053

Viero DP, Valipour M (2017) Modeling anisotropy in free-surface overland and shallow inundation flows. Adv Water Resour 104(Suppl C):1–14. https://doi.org/10.1016/j.advwatres.2017.03.007

Waltham T, Bell FG, Culshaw MG (2005) Sinkholes and subsidence: Karst and Cavernous rocks in engineering and construction. Springer, Berlin

Yao B, Mao X, Zhang K, Cai W (2012) A non-linear fluid–solid coupling mechanical model study for paleokarst collapse breccia pipes under erosion effect. Electron J Geotech Eng 17:277–290

Zidane A, Zechner E, Huggenberger P, Younes A (2014) On the effects of subsurface parameters on evaporite dissolution (Switzerland). J Contam Hydrol 160:42–52